Photochemical Behavior of Microbial Extracellular Polymeric Substances in the Aquatic Environment

Zhou, Shaofeng; Liao, Zhiyang; Zhang, Beiping; Hou, Rui; Wang, Yi; Zhou, Shungui; Zhang, Yifeng; Ren, Zhiyong Jason; Yuan, Yong

Published in:
Environmental Science & Technology (Washington)

Link to article, DOI:
10.1021/acs.est.1c02286

Publication date:
2021

Document Version
Peer reviewed version

Revision submitted to ***Environmental Science & Technology***

Photochemical Behavior of Microbial Extracellular Polymeric Substances in the Aquatic Environment

Shaofeng Zhou,[⊥] Zhiyang Liao,[⊥] Beiping Zhang, Rui Hou, Yi Wang, Shungui Zhou, Yifeng Zhang, Zhiyong Jason Ren, and Yong Yuan*

***Correspondence**: yuanyong@soil.gd.cn (Y. Yuan).

Authors Contributions

[⊥]S. Zhou and Z. Liao contributed equally to this paper.

Abstract

Microbially derived extracellular polymeric substances (EPS) occupy a large portion of dissolved organic matter (DOM) in surface waters, but the understanding of the photochemical behaviors of EPS is still very limited. In this study, the photochemical characteristics of EPS from different microbial sources (*Shewanella oneidensis, Escherichia coli,* and sewage sludge flocs) were investigated in terms of the production of reactive species (RS), such as triplet intermediates (^{3}EPS*), hydroxyl radicals (•OH), and singlet oxygen ($^1O_2$). The steady-state concentrations of •OH, ^{3}EPS*, and $^1O_2$ varied in the range of 2.55-8.73 × 10^{-17}, 3.01-4.56 × 10^{-15} and 2.08-2.66 × 10^{-13} M, respectively, which were within the range reported for DOM from other sources. The steady-state concentrations of RS varied among different EPS isolates due to the diversity of their composition. A strong photochemical degradation of the protein-like components in EPS isolates was identified by excitation emission matrix fluorescence with parallel factor analysis (EEM-PARAFAC), but relatively, humic-like components remained stable. Fourier-transform ion cyclotron resonance mass spectrometry (FT-ICR MS) further revealed that aliphatic portion of EPS was resistant to irradiation, while other portions with lower H/C ratios and higher O/C ratios were more susceptible to photolysis, leading to the phototransformation of EPS to higher saturation and lower aromaticity. With the phototransformation of EPS, the RS derived from EPS could effectively promote the degradation of antibiotic tetracycline. The findings of this study provide new insights into the photoinduced self-evolution of EPS and the interrelated photochemical fate of contaminants in the aquatic environment.

Keywords: extracellular polymeric substances, reactive species, triplet intermediates, phototransformation, tetracycline, dissolved organic matter

Synopsis: Extracellular polymeric substances show great photochemical activity for inducing their phototransformation and driving degradation of organic pollutants.

42 **TOC**

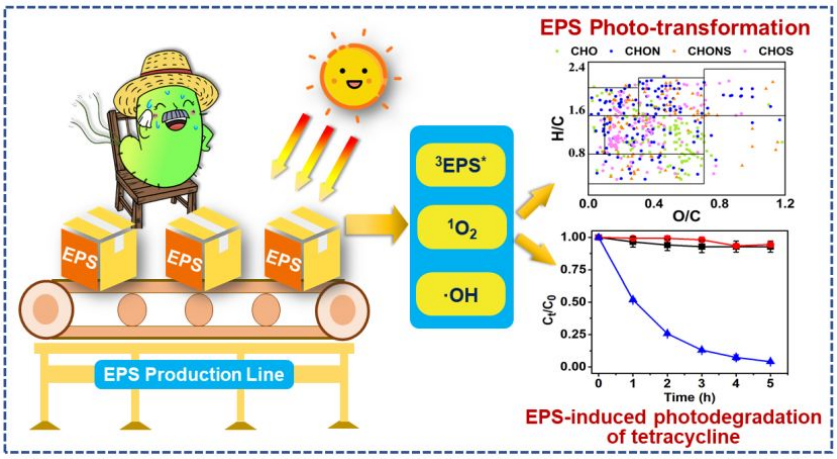
EPS Photo-transformation
CHO
CHON
CHONS
CHOS
H/C
O/C
EPS
EPS
EPS
EPS Production Line
$^3EPS^*$
$^1O_2$
·OH
C_t/C_0
Time (h)
EPS-induced photodegradation of tetracycline

43

44

■ INTRODUCTION

Extracellular polymeric substances (EPS) secreted from biological processes are a significant source of dissolved organic matter (DOM) ubiquitous in both terrestrial and aqueous environments.[1] It has been reported that greater than 40% of the total DOM in marine environment consists of EPS.[2] EPS is a complex mixture of polymers that primarily contain proteins, polysaccharides, humic substances and DNA.[3] Recently studies have discovered the important effects of EPS on biofilm adhesion,[4] quorum sensing/quenching,[5, 6] mass/electrons transference[7-9] and the self-protection of cells[10, 11]. In addition, EPS is also a source of the natural carbon pool in water systems and ubiquitously participates in various bio- and chemical reactions in the aquatic environments. Therefore, it is imperative to gain more understanding of the environmental impacts of EPS.

DOM is an active photosensitizer that may undergo a series of reactions triggered upon sunlight illumination. Owing to the absorption of photons, DOM could be photoactivated to form its triplet-excited state DOM (^{3}DOM*), which is one of the important sources for the further generation of reactive radical species, such as hydroxyl radicals (•OH) and singlet oxygen ($^1O_2$).[12-17] The potential photoactivity of DOM provides new insights into the process of natural carbon circulation, yet the photochemical behaviors of EPS and their environmental implications are largely uncharacterized in spite of the fact that EPS is a main DOM discharged into waterbody from wastewater utilities. As one of the most active moieties in EPS, humic substances have been shown to be susceptible to natural sunlight.[18-20] Attempts have been made to investigate the effects of EPS on the valence alternation of metal ions. For instance, the positive effects of EPS on silver nanoparticle formation from Ag^+ has been shown to occur

under both visible-light and ultraviolet irradiation.[2] In this case, light-induced hydrated electrons (reducing agents) could be activated from functional groups, such as aromatic compounds, hydroxyls and phenolic-OH of humic substances in the reduction of silver ions.[2] Previous work has also advanced photochemistry research in EPS,[21] but they only evaluated EPS as a mixture of photosensitive clusters in which functional groups and distinct subcomponents may affect the photoproperties. The phototransformation of EPS at the molecular level is largely unknown, so the understanding of the correlation between EPS photochemical behaviors and their associated environmental implications are needed.

This study isolated three types of EPS from pure culture *Shewanella oneidensis* MR-1, *Escherichia coli*, and mixed culture sewage sludge flocs (termed M-EPS, E-EPS and S-EPS, respectively) and compared them as research models to test the following research hypotheses: (1) how photochemical behavior of EPS vary among different sources; (2) to what extent does an EPS respond under sunlight illumination at the molecular level; and (3) how do these soluble microbial productions that act as light harvesters function on the attenuation of contaminants that co-exist in aquatic environments? Specifically, the phototransformation of EPS was revealed via a suite of mass spectrometry and fluorescence analyses. Additional investigation with regards to the possible reaction mechanisms between EPS and an antibiotic that co-exist in aquatic environment was also conducted and discussed.

■ MATERIALS AND METHODS

EPS Extraction. The chemicals used for all the experiments were provided in the Supporting Information, S1. Microbial EPS from *S. oneidensis* and *E. coli* were collected using a modified

heating extraction. Briefly, the cultured bacteria solutions (Supporting Information, S1) were used for bacterial pellets harvest after 24 h of cultivation using duplicate centrifugations (4500 × g, 5 min) to remove the residual medium prior to re-suspension in 50 mM phosphate buffer and heated in a water bath at 60℃ for 30 min. Then the supernatant was obtained as a raw EPS solution using a final centrifugation at 10, 000 × g for another 25 min. To remove the unsettled cells and residual salts, the solutions were filtered through 0.22-μm membrane filters and dialyzed in several dialysis bags (500 Da, MD 34, Union Carbide, U.S.A.) in sequence. The EPS from the sewage sludge (S-EPS) was collected following the same procedure, except for the bacterial cultivation. All of the EPS solutions were stored in the dark at 4 ℃ prior to use.

EPS Characterization. The procedures for EPS compositions (proteins, humic substances and polysaccharide) analysis were described in Supporting Information, S2. The total organic carbon (TOC) contents of the EPS samples were measured using a TOC analyzer (TOC-L CPH, Shimadu, Japan). A fluorescence spectrophotometer (FLS 1000, Edinburgh Instruments, U.K.) was used to obtain the three-dimensional excitation-emission matrix (EEM) fluorescence spectroscopic results for analyzing possible structure changes of the three EPS samples (Supporting Information, S3). Specific ultraviolet absorbance at 254 nm ($SUVA_{254}$, the ratio of absorbance at 254 nm to TOC concentration) and Fluorescence index (FI, the ratio of Intensity at Ex/Em = 370/470 to Intensity at Ex/Em = 370/520) were also calculated. A parallel factor (PARAFAC) analysis was conducted on the MATLAB 2017 software, as previously reported.[22] The freeze-dried EPS samples were mixed with KBr for Fourier transform infrared spectroscopy (FTIR) measurements, using an FTIR spectrometer (Nicolet 6700, Thermo-Fisher, USA.).

Photochemical Characterizations. A cylindrical quartz vessel (100 mL in total volume) with a water-circulating jacket was employed for all of the photochemical analyses (Figure S1). EPS solution samples were prepared at 50 mL aliquots with a concentration of 20 mg C/L. In addition, EPS solution was further diluted to 10 mg C/L for the detection of triplet intermediates involving 2,4,6-trimethylphenol (TMP), because this TMP has been reported sensitive to dissolved organic carbon.[23] The vessel was sealed after it was flushed with nitrogen gas to maintain an oxygen-free headspace during triplet intermediates detection. Natural sunlight was simulated using a 300 W Xenon lamp system (XE300, Redmatrix Co., China). The illumination below a wavelength of 280 nm was blocked using a light filter (ZJB280, Fulei Co., China). The intensity of the light (7.2×10^{-7} einstein L^{-1} s^{-1}) was confirmed using a ferrioxalate actinometer.[24] The light source was vertically settled at a distance of 20 cm above the liquid surface. The temperature of the irradiation solutions was maintained at 30 ^{o}C.

RS Detection. An electron paramagnetic resonance (EPR) analysis (EMXplus, Bruker, Germany) was conducted for the detection of RS in illumination process. The 5,5-dimethyl-1-pyrroline-oxide (DMPO) and 2,2,6,6-tetramethylpiperidine (TEMP) (both prepared in 100 mM) were employed as spin-trapping agents for •OH and $^1O_2$, respectively (Scheme S1). The yields of $^1O_2$ and the triplet reactive intermediates (termed ^{3}EPS*, in this case) were quantified by the consumption of furfuryl alcohol (FFA, 0.2 mM at the initial concentration) and TMP (1 mM at the initial concentration), respectively,[12, 25] which was determined using the HPLC (Essentia LC-16, Shimadzu Co., Japan). Terephthalate (TPA), a non-fluorescent probe compound, with an initial concentration of 1 mM, was used for detecting the formation of •OH.[12] The calculations of the steady state •OH, $^1O_2$, and ^{3}EPS* concentrations are detailed in Supporting

Information, S4. The quantum yields (Φ) of ^{3}EPS*, •OH, and $^1O_2$ were calculated using the following equations, modified from previously work by D. Wan et al.[12]

$$\Phi_i = R_i/R_a \quad (1)$$

$$R_a = \sum_{\lambda=280}^{700} E_P^0 (1\text{-}10^{-\varepsilon b[EPS]}) \quad (2)$$

Where R_i (mol L^{-1} s^{-1}) is the yield rate of RS (i = ^{3}EPS*, •OH, or $^1O_2$), R_a (Einstein L^{-1} s^{-1}) is the rate of light adsorption, E_P^0 (Einstein cm^{-2} s^{-1}) is the spectra photon irradiance which was calculated by intensity of the light (7.2×10^{-7} Einstein L^{-1} s^{-1}) multiplying the depth of water (3 cm). The *[EPS]* is the TOC value of EPS (10 mg L^{-1} for ^{3}EPS* or 20 mg L^{-1} for •OH, or $^1O_2$), *b* (cm) is the length of light path and ε (L mg^{-1} cm^{-1}) is the absorption coefficient of EPS at a specific wavelength.

Ultrahigh-resolution ESI FT-ICR MS Analysis. The EPS samples extracted before and after 5 h of illumination were analyzed using Fourier transform ion cyclotron resonance mass spectrometry (FT-ICR MS) equipped with a 9.4 T conducting magnet (Bruker Daltonics, Germany) coupled to an electrospray ionization source (ESI) in negative mode. The detailed procedure of the sample extraction is presented in Supporting Information, S5. The samples were injected at 180 μL/h. The FT-ICR MS operation was followed by the procedure previously described.[26] Detected peaks that had a signal-to-noise ratio (S/N) ≥ 5 and a mass accuracy of ≤ 0.6 ppm were imported for correcting the molecular formulas. The peaks that were found in the blank samples were excluded. Data processing and analysis were performed in Compass DataAnalysis 5.0 (Bruker). As salts were excluded in the pretreatments, the formulas that contained carbon (C), hydrogen (H), oxygen (O), nitrogen (N), and sulfur (S) were interpreted in this work. Data calculations were described in Supporting Information, S5

and the chemical rules for the formulas generations were followed the previously provided instructions.[27]

Tetracycline (TC) Degradation and Transformation Products. A total of 40 mg/L of tetracycline (TC) was prepared along with the M-EPS solution mentioned above. A 0.5-mL aliquot of each sample was mixed with 0.5 mL of methanol for determination of the TC concentration via high-performance liquid chromatography (HPLC). Quenching experiments were conducted with the addition of 20 mM of *tert*-butyl alcohol for •OH and nitrogen gas for $^1O_2$. All of the solutions were prepared at a pH of 7.0 ± 0.3 without buffer and continuously stirred at 300 rpm during the tests. All of the experiments were conducted in triplicate. The procedures for determination of the TC concentration and its transformation intermediates are described in Supporting Information, S6.

■ RESULTS AND DISCUSSION

Composition Properties of the EPS Isolates Varied from Different Sources. The EPS isolates obtained from the three different sources showed various contents of main components such as proteins, humic substances and polysaccharides. Specifically, the S-EPS showed the highest humic substance (15.7 mg/L) and the lowest protein content (6.36 mg/L), while M-EPS had the highest protein (19.36 mg/L) and lowest humic substance (5.39 mg/L) content (Table 1). $SUVA_{254}$ was used to evaluate the aromaticity of EPS samples, and the results indicated S-EPS had highest aromaticity based on the highest $SUVA_{254}$ values among all EPS samples (Table 1) while the differences in fluorescence index (FI) values of three EPS samples potentially indicated different compositions or chemical structure in humic substances.[28, 29] The

fluorescence analysis provided more details on the composition properties of the EPS isolates. Separated regions of each composition visualized in the EEM spectra are classified in Figure S2 and Table S1. The fluorescence signals showed the existence of aromatic-amino substances like tyrosine (Ex/Em of 225/300) in region I and II of the EEM spectra for S-EPS and M-EPS,[30] but this could be barely recognized in the E-EPS. The highest fluorescence signals of region I and II were found in the S-EPS sample as the aromatic protein-like substances, which is consistent to previous reports that such components were responsible for the stability of microbial structures.[31] The fluorescence signals at Ex/Em of 350/450 nm and 275/410 nm were attributed to a visible humic-like peak and UV humic-like peak[32], respectively. Although there was little difference in the peak intensity of the visible humic-like substances among the three EPS samples, both S-EPS and E-EPS contained more UV humic-like substance that basically composed of hydrophobic acids. Furthermore, the E-EPS sample also showed the strongest intensity of peak E in region III (Ex/Em of 235/410), which could be assigned to fulvic-like substance.[31] Thus, this diversity in composition might potentially contribute to the different photochemical behaviors of each EPS.

EPS Efficiently Produced Reactive Species (RS) under Illumination. The photochemical activity of the studied EPS samples was investigated by using probe molecules (HTPA, FFA and TMP) for •OH, $^1O_2$, and ^{3}EPS* detection, respectively. Figure 1 shows the concentration variations of the three probing agents as a function of irradiation time for the accumulation and kinetics of RS in the EPS solutions. As shown in Figure 1a, the S-EPS accumulated a larger portion of HTPA (1.28 μM) and leveled off gradually during illumination. However, a peak in the HTPA concentration in the third hour was identified in both M-EPS and E-EPS solutions

(0.32 and 0.63 μM, respectively), while in S-EPS solution the HTPA concentration continued increasing throughout irradiation tests. Though small part of HTPA might undergo direct photolysis upon extended irradiation, it is still reasonable to conclude that S-EPS was more responsive than its counterparts in the generation of •OH (Figure 1d and Table 1). It is known that the generation of •OH has a close relationship with hydrophilic humic substance which was known as a good source for •OH with high photoacticity,[33] so the lowest $[•OH]_{ss}$ in M-EPS could be explained by the limited humic substance concentration as indicated in the EEM spectra (Figure S2). Interestingly, although E-EPS presented lower $[•OH]_{ss}$ than S-EPS, the Φ (•OH) of the E-EPS was slightly higher than that of S-EPS (Table 1), indicating that •OH precursor in E-EPS was more photo-sensitive so as to form more •OH via the adsorption of per photon. While the lower $[•OH]_{ss}$ in E-EPS was explicable that some proteins, they might potentially be an extra sink of •OH along with other organic matters in EPS.[32] The photo-induced generation of •OH from EPS was further confirmed by EPR spectra using DMPO as the probe molecule. As presented in Figure S3a, the peaks corresponding to the DMPO-•OH adducts with a typical intensity ratio of 1:2:2:1 were clearly recognized in all the EPS solutions, providing the evidence of •OH presence in the system.[12] In contrast, no such signals were found in the group without EPS. Although the exact mechanisms of •OH formation from triplets as precursors are not yet fully understood,[12] the two pathways that involve the oxidation process of OH^- and/or abstraction of an H atom from water or direct photolysis from H_2O_2 generated by irradiated DOM are still under debate.[23, 34] In our case, the H_2O_2-related pathway was not significant, as illustrated in Figure S4. The catalase was used to quench H_2O_2 to diminish the H_2O_2 impact on •OH generation. Although decreases in $[•OH]_{ss}$ were observed in all three EPS

221 samples in the presence of catalase (Figure S4a), the H_2O_2-related pathway was contributed to
222 23.4%-27.9% of $[•OH]_{ss}$ in EPS solutions (Figure S4b).

223 For singlet oxygen generation, in the initial stages there was a slightly faster production of
224 $^1O_2$ (in loss of FFA) in the M-EPS than that in the E-EPS (Figure 1b), which was converse to
225 the •OH yield. Note that in the EEM spectra (Figure S2), the M-EPS was advantageous in
226 proteins content and specifically rich in aromatic proteins/amino acids, such as tryptophan and
227 tyrosine (regions I and II in the EEM)[35]. These constituents, basically, were shown to be active
228 sources where $^1O_2$ was photoexcited.[12, 32] The same conclusion is also applicable to the yield
229 of $^1O_2$ in the S-EPS obtained from its EEM spectra with the highest fluorescence intensity in
230 regions I and II (Figure S2). This resulted in the highest $[^1O_2]_{ss}$ at 2.66×10^{-13} M compared
231 with those of the M-EPS and E-EPS (2.08×10^{-13} and 2.11×10^{-13} M, respectively) (Table 1).
232 This finding was in accordance with the quantum yields of $^1O_2$ in other types of DOM (Table
233 S2), indicating that EPS was an appropriate photosensitizer that might share a similar process
234 for $^1O_2$ generation with other DOM. The generation of $^1O_2$ from EPS was also confirmed by
235 EPR spectra with TEMP as the probe molecule. The characteristic triplet spectrum with equal
236 intensities (1:1:1) was clearly observed in the EPS-TEMP solution of the three EPS samples
237 (Figure S3b), corresponding to oxidized TMPO by $^1O_2$.[36] This intuitively evidenced that EPS
238 could be photo-triggered to the production of singlet oxygen. Since the $^1O_2$ generation mainly
239 involved energy-transfer process with an energy gap of 94 kJ/mol,[37] the difference in energy-
240 transfer capabilities within three EPS samples need to be extracted. In this case, energy
241 distributions in EPS triplets were examined in the presence of high concentration of sorbic
242 alcohol (SA, i.e., 2,4-hexadienoic alcohol) as a high-energy triplet quencher (E_p > 250

kJ/mol).[38] An apparent $^1O_2$ quantum yield of high-energy EPS triplet ($\Phi_{H\text{-}EPS}$) and contribution (f_H) was calculated (eq 3 and 4) based on the loss of FFA in the presence of sorbic alcohol and results were presented in Figure S5.

$$f_H = \Phi_{H\text{-}EPS}/\Phi_{1_{O_2},EPS} \quad (3)$$

$$\Phi_{H\text{-}EPS} = \Phi_{1_{O_2},EPS} - \frac{d[FFA,SA]/dt}{\sum_{\lambda=280}^{700} E_P^0 (1 - 10^{-\varepsilon b[EPS]})} \quad (4)$$

Where $\Phi_{1_{O_2},EPS}$ is apparent $^1O_2$ quantum yield without sorbic alcohol, [FFA, SA] is the FFA concentration variation in the presence of sorbic alcohol. As shown in Figure S5, significant decreases were observed in the apparent $^1O_2$ quantum yield for all EPS samples after quenching by sorbic alcohol. The contribution of high-energy triplets for $^1O_2$ generation was calculated to be 55~70%, which was quite higher than those of terrestrial-origin DOM (~20%-38%) and comparable to those of effluent/wastewater organic matter (~65%).[38, 39] Thus, it could be suspected that EPS and effluent/wastewater organic matter triplets have a similar process of energy transfer to yield $^1O_2$. It was reported that aromatic ketone moieties within DOM were the main ingredients of higher-energy triplets.[38] A highest $\Phi_{H\text{-}EPS}$ of 70% was observed in the S-EPS solution, which was in accordance with the highest aromaticity among three EPS samples as revealed by the SUVA254. Meanwhile, the high-energy triplet states were dominant in S-EPS, which indicated that S-EPS might be more photochemical active relative to that of M-EPS and E-EPS.

The photogeneration of the triplet intermediates (^{3}EPS*) was also quantified using the reduction loss of TMP (Figure 1c). Note that this test was operated under oxygen-depleted condition since oxygen might act as a triplet quencher causing inaccurate assessment of triplets steady-state concentration and quantum yields (Figure S6). The order of quantum yields Φ

(^{3}EPS*) for the three EPS was E-EPS > S-EPS > M-EPS (Table 1), while the steady-state concentrations of ^{3}EPS* presented a slightly different trend. The $[^3EPS^*]_{ss}$ of the three EPS solutions were calculated as 3.68×10^{-13}, 4.56×10^{-13} and 3.01×10^{-13} M for M-EPS, E-EPS, and S-EPS, respectively. In contrast to •OH generation, there was little difference in the TMP loss between the M-EPS and E-EPS solutions, while the S-EPS presented the lowest triplet yield (Figure 1f). The triplet radicals could participate in photoreactions as a primary transient for the generation of •OH and $^1O_2$ via electron-transfer and energy-transfer reactions, respectively.[40, 41] Although the formation of $^1O_2$ is expected to be the primary photoreaction of triplet intermediates, as relatively low energy is required for starting deactivation of triplet intermediates by dissolved O_2.[25] However, this deactivation by oxygen was blocked since the solution was deaerated. Therefore, ^{3}EPS* was believed largely consumed for the generation of •OH, leading to the lowest $[^3EPS^*]_{ss}$ detected in the S-EPS. Other than •OH, $^1O_2$, and ^{3}EPS*, the possible generation of another important RS (superoxide radicals, O_2^-) was also investigated. However, there was no remarkable O_2^- detected during EPS illumination, which was discussed in Supporting Information, S7.

The structure of EPS was Significantly Altered by Illumination. It appeared that simulated solar irradiation could not significantly lead to mineralization of EPS because the averaged TOC removal efficiencies of the three EPS solutions were less than 10% (Figure S7). Thus, further analysis was conducted to reveal the phototransformation of EPS. The EEM spectra provided primary information on the phototransformation of EPS (Figure S2). The decay of the fluorescence intensity in regions I and II of all three EPS samples indicated a probable decomposition fate of such aromatic proteins during illumination. However, the fluorescence

intensities at Ex/Em = 350/450 (humic parts) barely decreased, except for that of E-EPS. It is reasonable to hypothesize that the photosensitivity of EPS was attributed to only certain parts. As such, the variations of main compositions in the EPS during illumination were further detailed using a PARAFAC analysis. As illustrated in Figure 2 (a-f), three main components (component 1 at Ex/Em = 220/320 nm and 280/320 nm, component 2 at Ex/Em = 280/350 nm and component 3 at Ex/Em = 250/460 and 300/460) were identified by the EEM-PARAFAC analysis. Among them, two components (components 1 and 2) were related to aromatic amino acids-like components (tyrosine-like and tryptophan-like components, respectively).[42, 43] These protein-like substances demonstrated a decreasing trend in all three EPS samples during illumination, confirming a strong photodegradation of such protein-like substances in EPS. It was not surprising that those highly aromatic substances could be oxidized due to their electron-rich moieties.[44] However, the component C was related to humic-like substances,[43] and its peak intensities remained relatively stable. The slight increase of component 3 in the M-EPS and S-EPS could be attributed to the formation of phenolic-like intermediates from the oxidation of the macro aromatic structure of other portions (e.g., aromatic proteins) in EPS.[45] Therefore, the contribution of those main components to the photoactivity of EPS was confirmed using the PARAFAC analysis.

The variations of FTIR spectra clearly provided the evolution of several EPS functional groups during illumination (Figure 2g~i). Three apparent oxygen-containing functional groups (C-O-C at 1080 cm^{-1}, C=O at 1620 cm^{-1}, and phenolic-OH at 1401 cm^{-1}) were recognized.[29, 46] In total, those functional groups experienced a decrease in both three EPS samples during illumination. It could be supportive that oxygen-containing compositions were sensitive to

irradiation and thus directed the photo-transformation of EPS to lower O/C and higher saturation. The phototransformation in the molecular compositions of the EPS samples after illumination was further analyzed using FT-ICR MS.

In general, the peak distributions of the EPS in the mass spectra taken before and after illumination showed similarities to some extent (Figure S8). Subsequently, compounds (isotopic isolates were not included) corresponding to the identified peaks (S/N $\geq$ 5) between 150 to 700 m/z were effectively visualized in the van Krevelen diagrams of the three EPS samples (Figure 3, Figure S9 and S10). The points in these diagrams were related to specific formulas that were classified into four major subcategories: CHO, CHON, CHONS, and CHOS compounds.[26, 47] Basically, these three sources of EPS shared similar subcategory compositions. Specifically, there was little difference on the abundance of CHON and CHONS compounds in the EPS samples. However, the abundance of CHOS compounds in M-EPS was higher than those in other two EPS samples, while CHO compounds went otherwise. According to Figure 3b, taking M-EPS as an example, selectivity was observed among different classes of organics during illumination. The CHOS compounds that contained C, H, O and S made up a relatively small proportion of the EPS, and its relative abundance continued to decrease after illumination. In particular, the disappearance of CHOS compounds primarily took place at lower H/C (< 1.5). Thus, these compounds with high levels of aromaticity could be more sensitive to photolysis. Although the relative abundances of the CHO compounds were able to remain stable, it was still difficult to tell whether this group was resistant to photocatalysis, as the CHO-contained formula could also be daughter intermediates from other groups. However, when comparing between the two van Krevelen diagrams, the CHO compounds showed a

tendency to move to a lower O/C structure, indicating unsaturated components with a high O/C could be more easily removed. Additionally, although they might be photolysis intermediates of other subcategories, there was also a possibility that they would experience losses of oxygen functional groups, as in dehydration.

According to previously reported rules for the boundaries of regions in the van Krevelen diagrams,[48, 49] these compounds in the four subcategories were divided into several regions as marked in Figure 3a, and their variations of contribution are summarized in Figure 3c. In general, decreases were revealed in the contributions of those classified as carbohydrates, aromatic structures, and CRAM-like classes, which were mostly from higher O/C or lower H/C regions. Specifically, CRAM-like groups are complex biopolymers that contain carbonyl species with isolated aliphatic ketones and several carboxyl groups.[26, 50] Considering that the loss of CHO compounds was largely observed in the CRAM-like regions and aromatic structures, it was speculated that unsaturated aliphatic acid was preferentially removed during the photolysis process of EPS.

In addition, the intensity weighted averaged (wa) values of X/C (X represents H, O, N, and S) and double bond equivalent (DBE) were further calculated and summarized in Table S3 and Text S5. The intensity weighted averaged values of the M-EPS samples were 1.409, 0.356, and 7.620 for H/C_{wa}, O/C_{wa}, and DBE/C_{wa}, respectively. Compared with those values (1.066, 0.497, and 9.450 or H/C_{wa}, O/C_{wa}, and DBE/C_{wa}, respectively) obtained from the NOM sample of the Suwannee River in another study,[26] the relatively lower O/C_{wa} and DBE/C_{wa} along with the higher H/C_{wa} strongly suggested there was more saturated matter in the M-EPS samples over the natural DOM. In contrast, the DBE/C_{wa} further decreased and a slightly higher H/C_{wa} was

observed in the M-EPS sample after illumination. This indicated that photoreactions in the EPS might be inclined to occur in aromatic, oxidized, and unsaturated components, which was consistent with the conclusions drawn from the van Krevelen diagrams. Similarly, the FT-ICR MS results of the E-EPS and S-EPS indicated that similar conclusions could be drawn regarding the photo-transformation process (Figure S9-S10 and Table S3). The direction from unsaturation to saturation of the EPS phototransformation process was confirmed.

The RS Generated from EPS could Induce the Degradation of Tetracycline. TC is considered as one of most consumed antibiotics that typically finds its way into natural environment through wastewater plant effluent.[51] In this study, the photocatalytic capacity of EPS on the transformation of TC was evaluated. As shown in Figure 4a, the direct photolysis mineralization of TC without EPS was quite difficult (an approximate 6.6% removal efficiency under 5 h of illumination) (Supporting Information, S8), and TC was also relatively stable with EPS in the dark (approximately a 7.2% loss in concentration). In contrast, the phototransformation of TC mediated by EPS was significantly enhanced, with nearly 95.7% of degradation. This suggested that the photochemical behaviors of EPS played a key role in this pollutant attenuation. The concentration loss of TC exhibited a pseudo-first-order kinetic with a rate constant (k_{obs}) of 0.644 ± 0.013 h^{-1} and a half-life period of 1.076 h (Figure 4), which were both were greater than those of groups without either illumination or the EPS addition.

The roles of each RS in the phototransformation of TC were further explored using a series of quenching experiments, and the results are presented in Figure S11. Compared with the group without any scavengers, the TC removal efficiencies were reduced by 11.6% and 28.5% in the presence of 20 mM *tert*-butyl alcohol (•OH quencher) and nitrogen gas (inhibit $^1O_2$

generation), respectively. The inhibition effects of TBA and nitrogen gas confirmed the nonnegligible effects of •OH and $^1O_2$ in the TC transformation. Comparatively, the TC degradation seemed more sensitive to the presence of $^1O_2$. Although •OH was featured in the non-selective reactions with most of contaminants,[52] the concentration of •OH was apparently several orders of magnitude lower than that of $^1O_2$, as aforementioned. That was because, as discussed above, the EPS itself acted as an •OH quencher that strongly inhibited the apparent yield and subsequently the oxidation capacity of •OH (Figure S12). In addition, $^1O_2$ has been reported as a typical electrophilic reactant that favorably attacks electron-rich organic substrates.[53, 54] In this context, the characteristic amino and phenolic-like structures in TC were probably favored and more vulnerable to the attack of $^1O_2$. In this case, ground-state oxygen served as terminal for energy transfer to form $^1O_2$,[53] but also a triplet quencher from the perspective of ^{3}EPS*.[12, 16, 55] The loss of oxygen, thereafter, led to the accumulation of ^{3}EPS* but simultaneous deficit of $^1O_2$, which lowered the TC degradation presented. In summary, singlet oxygen rather than the hydroxyl radical might contribute more in the photodegradation of TC. This trend was also consistent with that found in previous studies that have focused on other antibiotic isolates that underwent phototransformation in DOM-containing natural waters.[54]

The intermediates of TC formed during the illumination process were analyzed and identified using UPLC-Q-Orbitrap MS. Based on the mass spectra of these intermediates (Figure S13), the TC photoinduced transformation pathways were deciphered, as shown in Figure S14. First, the product 1 (P1, m/z 427) was generated via the dehydration of TC due to the attack of radicals. Instead of the loss of the hydroxyl in the carbon-ring C, as previous

397 studies have indicated,[56, 57] in this case, the hydroxyl located between rings A and B was
398 displaced according to the mass spectra of P2 (m/z 428). The molar mass of P2 was 1 Da higher
399 than that of P1, which was attributed to the replacement of the amino by an hydroxyl group at
400 ring A.[51] Notably, TC could be directly deaminated and oxidized without dehydration (P3 m/z
401 446). The $^1O_2$ acting as an electrophilic substance might be the key in the oxidation reaction,
402 since amino groups could be fragile due to their electron-rich property.[58] As shown in Figure
403 S14, the common fragments like 4-(dimethylamino)-2-formyl-3-hydroxybut-3-enal and 8,10-
404 dimethyl-3,4-dihydroanthracene-1,2-diol were detected, which were likely the follow-up
405 degraded compounds of P1-P3. Another primary transformation product (P4, m/z 462), a
406 hydroxylated product of TC,[59] was also identified. The double-bond at ring B was reported as
407 a susceptible site under the attack of •OH.[60] The product 5 (P4, m/z 437) was generated via the
408 N-demethylation of P4.[60, 61] Thus, the phototransformation of TC was enhanced by the RS
409 generated by the co-existed EPS during illumination.

410 **Environmental Implications.** This study characterized the photochemical behaviors of EPS
411 from three microbial sources, which is a significant component of effluent organic matters no
412 matter in natural and engineered surface waterbodies.[32] The pathways of natural EPS evolution
413 under solar illumination were summarized in Scheme 1. The EPS, as a photosensitizer similar
414 to DOM, could be photoactivated for RS generation (triplet intermediates, •OH, and $^1O_2$),
415 which accelerated the phototransformation of EPS.[21] At the molecular level, the EPS
416 components tended to evolve to lower aromatic structures and less oxygen-containing
417 functional groups. The photochemistry of EPS might contribute to the natural digestion of trace
418 organics co-existing in aquatic conditions. In this study, tetracycline was tested as a model

pollutant, as it is one of the most widely used antibiotics and is frequently found in downstream water systems primarily in the form of effluent from agricultural water effluent.[62, 63] TC could be effectively decomposed via the mediation of RS derived from EPS. Although the hybrid effects of illumination and EPS on contaminant removal is unlikely on par with the efficiency of normal water-remediation technologies (e.g., the advanced oxidation process), this process that mimics natural phototransformation could be of fundamental and practical interest, especially for the generation of RS. In water ecological systems, like estuaries and wetlands, that involve massive amounts of EPS,[64] the photochemical sensitivity of EPS will enhance the capability of natural attenuation of the waterbody, and open up new opportunities in research with regards to the transformation fate of natural organics. However, it must be pointed out that the photochemical activation of EPS may also stem from various metal ions, so further study is needed. One recent study presented a static and dynamic quenching theory regarding the suppression of prerequisite triplet radicals (the precursor of RS) caused by metal ions, and even heavy metal ions showed more detrimental effects.[12] Overall, the results of this study provide significant new insights on the unrecognized photochemical pathways of EPS, especially in natural waters, and it will direct further research in this important field.

■ ACKNOWLEDGMENTS

This work was supported by Natural Science Foundation of China (41877045, 21876032, 21906028 and 41907122).

■ SUPPORTING INFORMATION

Descriptions for chemicals, EPS compostions analysis, EPS fluorescence analysis, calculation of steady-state concentrations, sample extraction for FT-ICR MS, determination of TC concentration and its transformation, the discussion on superoxide radicals (O_2^{-}) and the degradation of TC via direct photolysis (Text S1-S8). Tables for identification priciples of EEM spectra, steady state concentraions comparison and profiles of intensity weighted averaged (wa) values (Table S1-S3). Scheme for photogeneration of radicals and their probing reactions (Scheme S1). Figures for experimental setup, EEM spectra, EPR spectra, comparisons of two •OH formation pathways, the effects of high-energy triplets on yield of singlet oxygen, comparisons of the yield of ^{3}EPS*, $[^3EPS^*]_{ss}$, quamtum yield of ^{3}EPS* in open-air or anaerobic conditions, TOC removal efficiencies, negative ion mass spectra of M-EPS, FT-ICR MS analysis of S-EPS and E-EPS, effects of scavengers on TC degradation, fluorescence intensity changes of S-EPS, mass spectra of TC and photo-transformation products and proposed pathways of TC (Figure S1-S14).

■ AUTHOR INFORMATION

Corresponding Author

Yong Yuan - *Guangdong Key Laboratory of Environmental Catalysis and Health Risk Control, School of Environmental Science and Engineering, Institute of Environmental Health and Pollution Control, Guangdong University of Technology, Guangzhou 510006, China;* Email: yuanyong@soil.gd.cn

Authors

Shaofeng Zhou - *Guangdong Key Laboratory of Environmental Catalysis and Health Risk*

Control, School of Environmental Science and Engineering, Institute of Environmental Health and Pollution Control, Guangdong University of Technology, Guangzhou 510006; China & Guangdong Provincial Key Laboratory of Microbial Culture Collection and Application, State Key Laboratory of Applied Microbiology Southern China, Institute of Microbiology, Guangdong Academy of Science, Guangzhou, 510070, China

Zhiyang Liao - *Guangdong Key Laboratory of Environmental Catalysis and Health Risk Control, School of Environmental Science and Engineering, Institute of Environmental Health and Pollution Control, Guangdong University of Technology, Guangzhou 510006, China*

Beiping Zhang - *Guangdong Key Laboratory of Environmental Catalysis and Health Risk Control, School of Environmental Science and Engineering, Institute of Environmental Health and Pollution Control, Guangdong University of Technology, Guangzhou 510006, China*

Rui Hou - *Guangdong Key Laboratory of Environmental Catalysis and Health Risk Control, School of Environmental Science and Engineering, Institute of Environmental Health and Pollution Control, Guangdong University of Technology, Guangzhou 510006, China*

Yi Wang - *Guangdong Key Laboratory of Environmental Catalysis and Health Risk Control, School of Environmental Science and Engineering, Institute of Environmental Health and Pollution Control, Guangdong University of Technology, Guangzhou 510006, China*

Shungui Zhou - *Fujian Provincial Key Laboratory of Soil Environmental Health and*

Regulation, School of Resources and Environment, Fujian Agriculture and Forestry, Fuzhou 350000, China

Yifeng Zhang - *Department of Environmental Engineering, Technical University of Denmark, DK-2800 Lyngby, Denmark*

Zhiyong Jason Ren - *Department of Civil and Environmental Engineering and Andlinger Center for Energy and the Environment, Princeton University, Princeton, NJ, 08544, USA*

■ REFERENCES

1. Derrien, M.; Brogi, S. R.; Goncalves-Araujo, R., Characterization of aquatic organic matter: Assessment, perspectives and research priorities. *Water Res.* **2019,** *163*, 17.

2. Zhang, X.; Yang, C.-W.; Yu, H.-Q.; Sheng, G.-P., Light-induced reduction of silver ions to silver nanoparticles in aquatic environments by microbial extracellular polymeric substances (EPS). *Water Res.* **2016,** *106*, 242-248.

3. Gerbersdorf, S. U.; Westrich, B.; Paterson, D. M., Microbial extracellular polymeric substances (EPS) in fresh water sediments. *Microbial Ecology* **2009,** *58*, (2), 334-349.

4. Harimawan, A.; Ting, Y.-P., Investigation of extracellular polymeric substances (EPS) properties of P. aeruginosa and B. subtilis and their role in bacterial adhesion. *Colloids and Surfaces B: Biointerfaces* **2016,** *146*, 459-467.

5. Jiang, B.; Liu, Y., Roles of ATP-dependent N-acylhomoserine lactones (AHLs) and extracellular polymeric substances (EPSs) in aerobic granulation. *Chemosphere* **2012,** *88*, (9), 1058-1064.

6. Kampouris, I. D.; Karayannakidis, P. D.; Banti, D. C.; Sakoula, D.; Konstantinidis, D.;

507 Yiangou, M.; Samaras, P. E., Evaluation of a novel quorum quenching strain for MBR
508 biofouling mitigation. *Water Res.* **2018,** *143*, 56-65.
509 7. Lin, Z.-Q.; Shao, W.; Xu, J.; Sheng, G.-P., Accurately quantifying the reductive capacity
510 of microbial extracellular polymeric substance by mediated electrochemical oxidation method.
511 *Science of The Total Environment* **2019,** *673*, 541-545.
512 8. Yan, L.; Zhang, M.; Liu, Y.; Liu, C.; Zhang, Y.; Liu, S.; Yu, L.; Hao, G.; Chen, Z.; Zhang,
513 Y., Enhanced nitrogen removal in an aerobic granular sequencing batch reactor under low DO
514 concentration: Role of extracellular polymeric substances and microbial community structure.
515 *Bioresource Technology* **2019,** *289*, 121651.
516 9. Zhou, S.; Huang, S.; He, J.; Li, H.; Zhang, Y., Electron transfer of Pseudomonas
517 aeruginosa CP1 in electrochemical reduction of nitric oxide. *Bioresource Technology* **2016,**
518 *218*, 1271-1274.
519 10. Yang, G.; Huang, L.; Yu, Z.; Liu, X.; Chen, S.; Zeng, J.; Zhou, S.; Zhuang, L., Anode
520 potentials regulate Geobacter biofilms: New insights from the composition and spatial structure
521 of extracellular polymeric substances. *Water Res.* **2019,** *159*, 294-301.
522 11. Zhang, L.; Dong, D.; Hua, X.; Guo, Z., Inhibitory effects of extracellular polymeric
523 substances on ofloxacin sorption by natural biofilms. *Science of The Total Environment* **2018,**
524 *625*, 178-184.
525 12. Wan, D.; Sharma, V. K.; Liu, L.; Zuo, Y.; Chen, Y., Mechanistic insight into the effect of
526 metal ions on photogeneration of reactive species from dissolved organic matter. *Environ. Sci.*
527 *Technol.* **2019,** *53*, (10), 5778-5786.
528 13. Leresche, F.; McKay, G.; Kurtz, T.; von Gunten, U.; Canonica, S.; Rosario-Ortiz, F. L.,

529 Effects of ozone on the photochemical and photophysical properties of dissolved organic
530 matter. *Environ. Sci. Technol.* **2019,** *53*, (10), 5622-5632.
531 14. Li, Y.; Chen, J.; Qiao, X.; Zhang, H.; Zhang, Y.-n.; Zhou, C., Insights into photolytic
532 mechanism of sulfapyridine induced by triplet-excited dissolved organic matter. *Chemosphere*
533 **2016,** *147*, 305-310.
534 15. Li, Y.; Wei, X.; Chen, J.; Xie, H.; Zhang, Y.-n., Photodegradation mechanism of
535 sulfonamides with excited triplet state dissolved organic matter: A case of sulfadiazine with 4-
536 carboxybenzophenone as a proxy. *Journal of Hazardous Materials* **2015,** *290*, 9-15.
537 16. Dalrymple, R. M.; Carfagno, A. K.; Sharpless, C. M., Correlations between dissolved
538 organic matter optical properties and quantum yields of singlet oxygen and hydrogen peroxide.
539 *Environ. Sci. Technol.* **2010,** *44*, (15), 5824-5829.
540 17. Maizel, A. C.; Li, J.; Remucal, C. K., Relationships between dissolved organic matter
541 composition and photochemistry in lakes of diverse trophic status. *Environ. Sci. Technol.* **2017,**
542 *51*, (17), 9624-9632.
543 18. Cavani, L.; Halladja, S.; ter Halle, A.; Guyot, G.; Corrado, G.; Ciavatta, C.; Boulkamh, A.;
544 Richard, C., Relationship between photosensitizing and emission properties of peat humic acid
545 fractions obtained by tangential ultrafiltration. *Environ. Sci. Technol.* **2009,** *43*, (12), 4348-
546 4354.
547 19. Rong, H.; Garg, S.; Waite, T. D., Impact of light and Suwanee River Fulvic Acid on O_2
548 and H_2O_2 Mediated Oxidation of Silver Nanoparticles in Simulated Natural Waters. *Environ.*
549 *Sci. Technol.* **2019,** *53*, (12), 6688-6698.
550 20. Yin, Y.; Liu, J.; Jiang, G., Sunlight-Induced reduction of ionic Ag and Au to metallic

551 nanoparticles by dissolved organic matter. *ACS Nano* **2012,** *6*, (9), 7910-7919.

552 21. He, H.; Han, F.; Sun, S.; Deng, H.; Huang, B.; Pan, X.; Dionysiou, D. D., Photosensitive

553 cellular polymeric substances accelerate 17α-ethinylestradiol photodegradation. *Chem. Eng. J.*

554 **2020,** *381*, 122737.

555 22. Sheng, G.-P.; Xu, J.; Luo, H.-W.; Li, W.-W.; Li, W.-H.; Yu, H.-Q.; Xie, Z.; Wei, S.-Q.;

556 Hu, F.-C., Thermodynamic analysis on the binding of heavy metals onto extracellular

557 polymeric substances (EPS) of activated sludge. *Water Res.* **2013,** *47*, (2), 607-614.

558 23. Berg, S. M.; Whiting, Q. T.; Herrli, J. A.; Winkels, R.; Wammer, K. H.; Remucal, C. K.,

559 The role of dissolved organic matter composition in determining photochemical reactivity at

560 the molecular level. *Environ. Sci. Technol.* **2019,** *53*, (20), 11725-11734.

561 24. Laszakovits, J. R.; Berg, S. M.; Anderson, B. G.; O'Brien, J. E.; Wammer, K. H.; Sharpless,

562 C. M., p-Nitroanisole/pyridine and p-nitroacetophenone/pyridine actinometers revisited:

563 quantum yield in comparison to ferrioxalate. *Environmental Science & Technology Letters*

564 **2017,** *4*, (1), 11-14.

565 25. Rosario-Ortiz, F. L.; Canonica, S., Probe compounds to assess the photochemical activity

566 of dissolved organic matter. *Environ. Sci. Technol.* **2016,** *50*, (23), 12532-12547.

567 26. Yuan, Z.; He, C.; Shi, Q.; Xu, C.; Li, Z.; Wang, C.; Zhao, H.; Ni, J., Molecular insights

568 into the transformation of dissolved organic matter in landfill leachate concentrate during

569 biodegradation and coagulation processes using ESI FT-ICR MS. *Environ. Sci. Technol.* **2017,**

570 *51*, (14), 8110-8118.

571 27. Subdiaga, E.; Harir, M.; Orsetti, S.; Hertkorn, N.; Schmitt-Kopplin, P.; Haderlein, S. B.,

572 Preferential sorption of tannins at aluminum oxide affects the electron exchange capacities of

573 dissolved and sorbed humic acid fractions. *Environ. Sci. Technol.* **2020,** *54*, (3), 1837-1847.
574 28. Croué, J. P.; Benedetti, M. F.; Violleau, D.; Leenheer, J. A., Characterization and copper
575 binding of humic and nonhumic organic matter isolated from the South Platte River: Evidence
576 for the presence of nitrogenous binding site. *Environ. Sci. Technol.* **2003,** *37*, (2), 328-336.
577 29. Dai, H.; He, H.; Lai, C.; Xu, Z.; Zheng, X.; Yu, G.; Huang, B.; Pan, X.; Dionysiou, D. D.,
578 Modified humic acids mediate efficient mineralization in a photo-bio-electro-Fenton process.
579 *Water Res.* **2021,** *190*, 116740.
580 30. Tan, B.; Zhou, S.; Wang, Y.; Zhang, B.; Zhou, L.; Yuan, Y., Molecular insight into
581 electron transfer properties of extracellular polymeric substances of electroactive bacteria by
582 surface-enhanced Raman spectroscopy. *SCIENCE CHINA Technological Sciences* **2019,** *62*,
583 (1674-7321), 1679.
584 31. Zhu, L.; Qi, H. Y.; Lv, M. L.; Kong, Y.; Yu, Y. W.; Xu, X. Y., Component analysis of
585 extracellular polymeric substances (EPS) during aerobic sludge granulation using FTIR and
586 3D-EEM technologies. *Bioresource Technology* **2012,** *124*, 455-459.
587 32. Zhang, D.; Yan, S.; Song, W., Photochemically induced formation of reactive oxygen
588 species (ROS) from effluent organic matter. *Environ. Sci. Technol.* **2014,** *48*, (21), 12645-
589 12653.
590 33. Lee, E.; Glover, C. M.; Rosario-Ortiz, F. L., Photochemical formation of hydroxyl radical
591 from effluent organic matter: role of composition. *Environ. Sci. Technol.* **2013,** *47*, (21), 12073-
592 12080.
593 34. Sur, B.; Rolle, M.; Minero, C.; Maurino, V.; Vione, D.; Brigante, M.; Mailhot, G.,
594 Formation of hydroxyl radicals by irradiated 1-nitronaphthalene (1NN): oxidation of hydroxyl

595 ions and water by the 1NN triplet state. *Photochem. Photobiol. Sci.* **2011,** *10*, (11), 1817-1824.
596 35. Chen, W.; Westerhoff, P.; Leenheer, J. A.; Booksh, K., Fluorescence excitation−emission
597 matrix regional integration to quantify spectra for dissolved organic matter. *Environ. Sci.*
598 *Technol.* **2003,** *37*, (24), 5701-5710.
599 36. Yin, R.; Guo, W.; Wang, H.; Du, J.; Wu, Q.; Chang, J.-S.; Ren, N., Singlet oxygen-
600 dominated peroxydisulfate activation by sludge-derived biochar for sulfamethoxazole
601 degradation through a nonradical oxidation pathway: Performance and mechanism. *Chem. Eng.*
602 *J.* **2019,** *357*, 589-599.
603 37. Ogilby, P. R., Singlet oxygen: there is indeed something new under the sun. *Chemical*
604 *Society Reviews* **2010,** *39*, (8), 3181-3209.
605 38. Wang, H.; Zhou, H.; Ma, J.; Nie, J.; Yan, S.; Song, W., Triplet photochemistry of dissolved
606 black carbon and its effects on the photochemical formation of reactive oxygen species.
607 *Environ. Sci. Technol.* **2020,** *54*, (8), 4903-4911.
608 39. Zhou, H.; Yan, S.; Lian, L.; Song, W., Triplet-state photochemistry of dissolved organic
609 matter: triplet-state energy distribution and surface electric charge conditions. *Environ. Sci.*
610 *Technol.* **2019,** *53*, (5), 2482-2490.
611 40. McNeill, K.; Canonica, S., Triplet state dissolved organic matter in aquatic photochemistry:
612 reaction mechanisms, substrate scope, and photophysical properties. *Environ. Sci.-Process*
613 *Impacts* **2016,** *18*, (11), 1381-1399.
614 41. Zhang, Y.; Del Vecchio, R.; Blough, N. V., Investigating the mechanism of hydrogen
615 peroxide photoproduction by humic substances. *Environ. Sci. Technol.* **2012,** *46*, (21), 11836-
616 11843.

617 42. Li, G.-F.; Huang, B.-C.; Cheng, Y.-F.; Ma, W.-J.; Li, S.-T.; Gong, B.; Guan, Y.-F.; Fan,
618 N.-S.; Jin, R.-C., Determination of the response characteristics of anaerobic ammonium
619 oxidation bioreactor disturbed by temperature change with the spectral fingerprint. *Science of*
620 *The Total Environment* **2020,** *719*, 137513.
621 43. Maqbool, T.; Hur, J., Changes in fluorescent dissolved organic matter upon interaction
622 with anionic surfactant as revealed by EEM-PARAFAC and two dimensional correlation
623 spectroscopy. *Chemosphere* **2016,** *161*, 190-199.
624 44. Nie, J.; Yan, S.; Lian, L.; Sharma, V. K.; Song, W., Development of fluorescence
625 surrogates to predict the ferrate(vi) oxidation of pharmaceuticals in wastewater effluents. *Water*
626 *Res.* **2020**, 116256.
627 45. Huang, G.; Xiao, Z.; Zhen, W.; Fan, Y.; Zeng, C.; Li, C.; Liu, S.; Wong, P. K., Hydrogen
628 production from natural organic matter via cascading oxic-anoxic photocatalytic processes: An
629 energy recovering water purification technology. *Water Res.* **2020,** *175*, 115684.
630 46. Zhang, B.; Zhou, S.; Zhou, L.; Wen, J.; Yuan, Y., Pyrolysis temperature-dependent
631 electron transfer capacities of dissolved organic matters derived from wheat straw biochar.
632 *Science of The Total Environment* **2019,** *696*, 133895.
633 47. Dvorski, S. E. M.; Gonsior, M.; Hertkorn, N.; Uhl, J.; Müller, H.; Griebler, C.; Schmitt-
634 Kopplin, P., Geochemistry of dissolved organic matter in a spatially highly resolved
635 groundwater petroleum hydrocarbon plume cross-section. *Environ. Sci. Technol.* **2016,** *50*, (11),
636 5536-5546.
637 48. Yu, Z.; Liu, X. M.; Chen, C. Y.; Liao, H. P.; Chen, Z.; Zhou, S. G., Molecular insights into
638 the transformation of dissolved organic matter during hyperthermophilic composting using ESI

639 FT-ICR MS. *Bioresource Technology* **2019,** *292*, 5.

640 49. Krevelen, D. W., Graphical-statistical method for the study of structure and reaction
641 processes of coal. *Fuel* **1961,** *29*, 269-283.

642 50. Smith, C. R.; Sleighter, R. L.; Hatcher, P. G.; Lee, J. W., Molecular characterization of
643 inhibiting biochar water-extractable substances using electrospray ionization fourier transform
644 ion cyclotron resonance mass spectrometry. *Environ. Sci. Technol.* **2013,** *47*, (23), 13294-
645 13302.

646 51. Llorca, M.; Rodríguez-Mozaz, S.; Couillerot, O.; Panigoni, K.; de Gunzburg, J.; Bayer, S.;
647 Czaja, R.; Barceló, D., Identification of new transformation products during enzymatic
648 treatment of tetracycline and erythromycin antibiotics at laboratory scale by an on-line
649 turbulent flow liquid-chromatography coupled to a high resolution mass spectrometer LTQ-
650 Orbitrap. *Chemosphere* **2015,** *119*, 90-98.

651 52. Shemer, H.; Sharpless, C. M.; Elovitz, M. S.; Linden, K. G., Relative rate constants of
652 contaminant candidate list pesticides with hydroxyl radicals. *Environ. Sci. Technol.* **2006,** *40*,
653 (14), 4460-4466.

654 53. Tratnyek, P. G.; Hoigne, J., Oxidation of substituted phenols in the environment: a QSAR
655 analysis of rate constants for reaction with singlet oxygen. *Environ. Sci. Technol.* **1991,** *25*, (9),
656 1596-1604.

657 54. Yang, W. L.; Ben Abdelmelek, S.; Zheng, Z.; An, T. C.; Zhang, D. N.; Song, W. H.,
658 Photochemical transformation of terbutaline (pharmaceutical) in simulated natural waters:
659 Degradation kinetics and mechanisms. *Water Res.* **2013,** *47*, (17), 6558-6565.

660 55. Zhou, Z.; Chen, B.; Qu, X.; Fu, H.; Zhu, D., Dissolved black carbon as an efficient

661 sensitizer in the photochemical transformation of 17β-estradiol in aqueous solution. *Environ.*
662 *Sci. Technol.* **2018,** *52*, (18), 10391-10399.
663 56. Li, Z.; Guo, C.; Lyu, J.; Hu, Z.; Ge, M., Tetracycline degradation by persulfate activated
664 with magnetic Cu/CuFe2O4 composite: Efficiency, stability, mechanism and degradation
665 pathway. *Journal of Hazardous Materials* **2019,** *373*, 85-96.
666 57. Solliec, M.; Roy-Lachapelle, A.; Sauvé, S., Quantitative performance of liquid
667 chromatography coupled to Q-Exactive high resolution mass spectrometry (HRMS) for the
668 analysis of tetracyclines in a complex matrix. *Analytica Chimica Acta* **2015,** *853*, 415-424.
669 58. Xu, L.; Li, H.; Mitch, W. A.; Tao, S.; Zhu, D., Enhanced phototransformation of
670 tetracycline at smectite clay surfaces under simulated sunlight via a lewis-base catalyzed
671 alkalization mechanism. *Environ. Sci. Technol.* **2019,** *53*, (2), 710-718.
672 59. Zhang, Y.; Zhou, J.; Chen, J.; Feng, X.; Cai, W., Rapid degradation of tetracycline
673 hydrochloride by heterogeneous photocatalysis coupling persulfate oxidation with MIL-53(Fe)
674 under visible light irradiation. *Journal of Hazardous Materials* **2020,** *392*, 122315.
675 60. Han, C.-H.; Park, H.-D.; Kim, S.-B.; Yargeau, V.; Choi, J.-W.; Lee, S.-H.; Park, J.-A.,
676 Oxidation of tetracycline and oxytetracycline for the photo-Fenton process: Their
677 transformation products and toxicity assessment. *Water Res.* **2020,** *172*, 115514.
678 61. Leng, Y.; Bao, J.; Chang, G.; Zheng, H.; Li, X.; Du, J.; Snow, D.; Li, X., Biotransformation
679 of tetracycline by a novel bacterial strain Stenotrophomonas maltophilia DT1. *Journal of*
680 *Hazardous Materials* **2016,** *318*, 125-133.
681 62. Jia, J.; Cheng, M.; Xue, X.; Guan, Y.; Wang, Z., Characterization of tetracycline effects
682 on microbial community, antibiotic resistance genes and antibiotic resistance of Aeromonas

683 spp. in gut of goldfish Carassius auratus Linnaeus. *Ecotoxicology and Environmental Safety*
684 **2020,** *191*, 110182.
685 63. Ghirardini, A.; Grillini, V.; Verlicchi, P., A review of the occurrence of selected
686 micropollutants and microorganisms in different raw and treated manure – Environmental risk
687 due to antibiotics after application to soil. *Science of The Total Environment* **2020,** *707*, 136118.
688 64. Flemming, H.-C.; Wingender, J., The biofilm matrix. *Nature Reviews Microbiology* **2010,**
689 *8*, (9), 623-633.
690
691

692 **Table 1** Composition properties, RS steady-state concentrations and quantum yields of the
693 three EPS samples.
694

	M-EPS	E-EPS	S-EPS
Proteins (mg/L)	19.36 ± 1.26	11.43 ± 0.58	6.36 ± 0.67
Polysaccharides (mg/L)	15.23 ± 0.86	17.28 ± 0.74	19.25 ± 0.99
Humic substances (mg/L)	5.39 ± 0.59	6.77 ± 0.44	15.70 ± 1.32
$SUVA_{254}$	2.81 ± 0.71	1.32 ± 0.59	4.43 ± 0.97
FI	0.69 ± 0.09	1.52 ± 0.11	1.31 ± 0.24
$[\bullet OH]_{ss}$ (10^{-17} M)	2.55 ± 0.26	5.18 ± 0.42	8.73 ± 0.38
$[^1O_2]_{ss}$ (10^{-13} M)	2.08 ± 0.21	2.11 ± 0.18	2.66 ± 0.42
$[^3EPS^*]_{ss}$ (10^{-15} M)	3.68 ± 0.33	4.56 ± 0.48	3.01 ± 0.61
Φ (•OH) (10^{-5})	0.43 ± 0.05	2.20 ± 0.19	1.94 ± 0.12
Φ ($^1O_2$) (10^{-2})	4.01 ± 0.33	4.08 ± 0.29	7.40 ± 0.18
Φ ($^3EPS^*$) (10^{-4})	3.74 ± 0.28	11.71 ± 0.72	3.90 ± 0.22

695

Figure 1

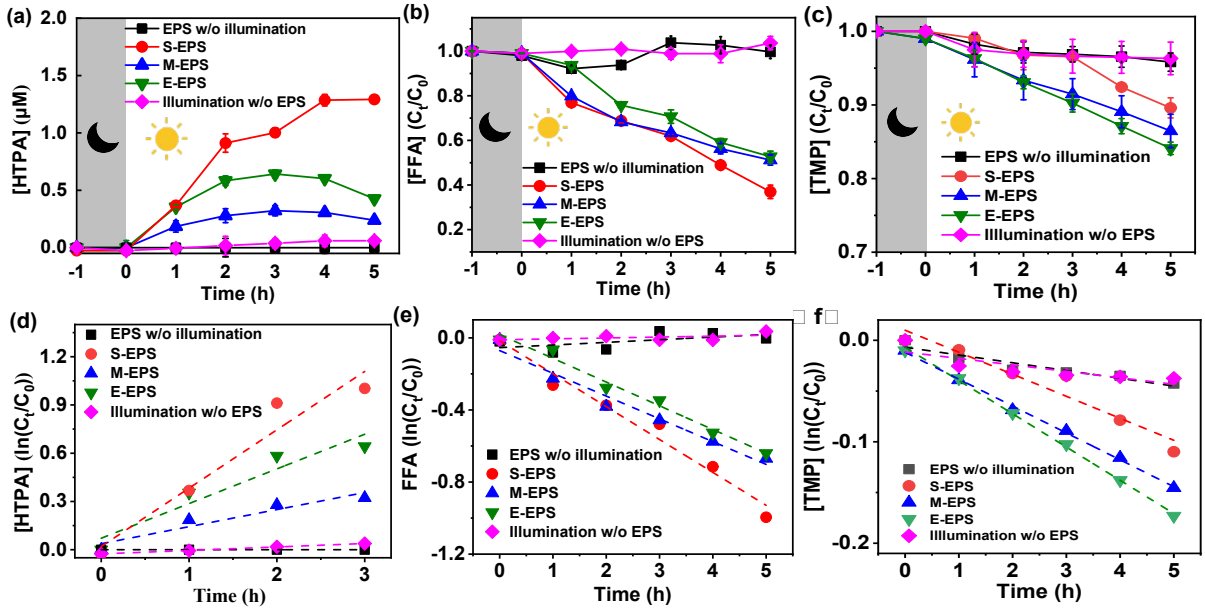

Figure 1 (a) Hydroxyl radical (•OH) generation (in the form of HTPA increase) and the depletion of (b) FFA and (c) TMP, indicating the generation of singlet oxygen ($^1O_2$) and triplet intermediates (^{3}EPS*), respectively, as a function of irradiation time C_t and C_0 were the FFA or TMP concentrations at before and after illumination, respectively. (d) ~ (f) First order kinetics of the •OH, $^1O_2$ and ^{3}EPS* generation, respectively. ($[EPS]_{initial}$ = 20 mg TOC /L, $[FFA]_{initial}$ = 0.2 mM, $[TPA]_{initial}$ = $[TMP]_{initial}$ = 1 mM. Note that $[EPS]_{initial}$ was diluted to 10 mg TOC/L and the reactor was kept in oxygen-deleted condition for TMP experiment.

Figure 2

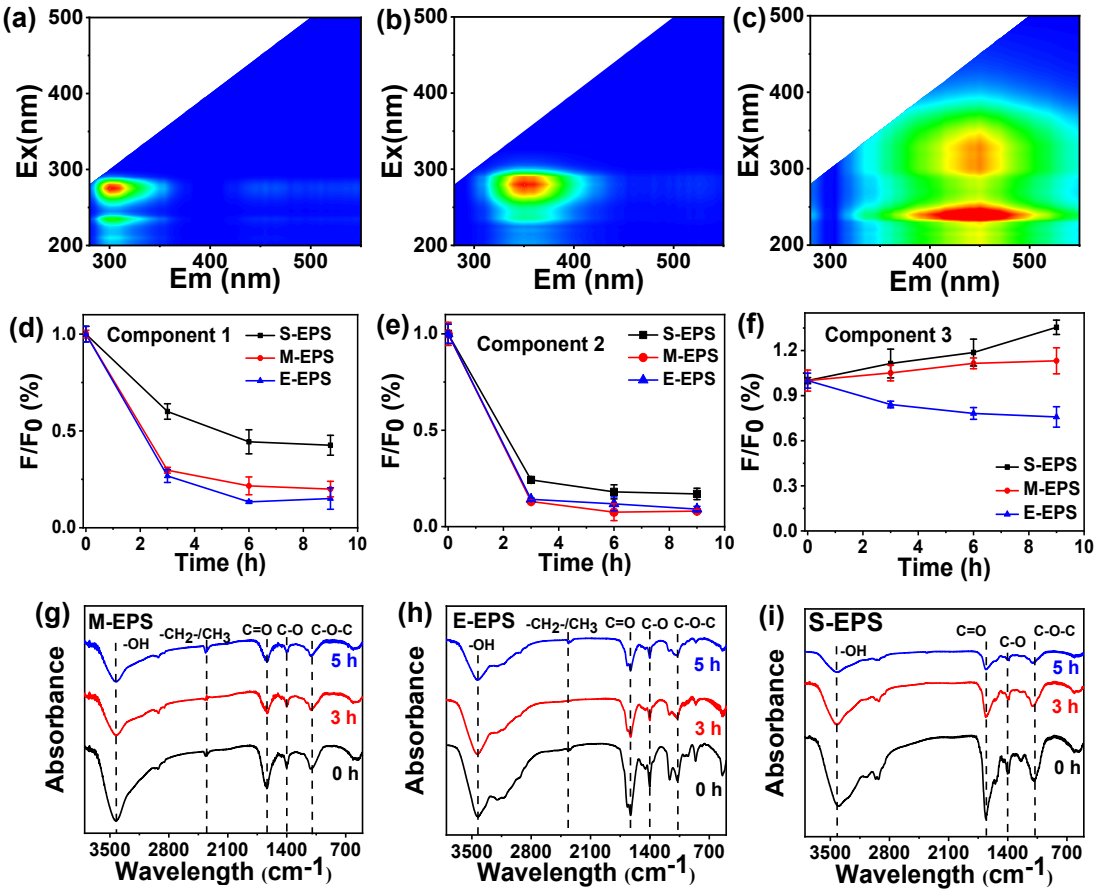

Figure 2 (a)~(c) The EEM spectra of three main components (1, 2 and 3, respectively) in EPS extracted from PARAFAC analysis, (d)~(f) their corresponding peaks intensities of the EEM spectra at different illumination time, and changes in FTIR spectra of EPS samples with increasing illumination time. (g) *S. oneidensis* EPS, (h) *E. coli* EPS and (i) Sludge EPS.

Figure 3

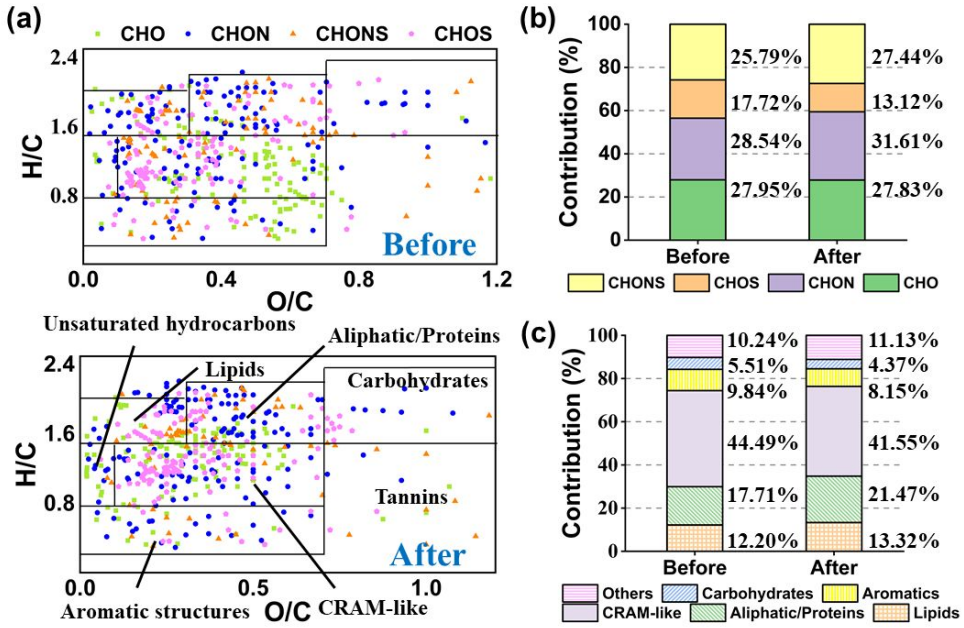

Figure 3 (a) Van Krevelen diagrams of CHO, CHON, CHOS, CHONS of M-EPS compositions before and after illumination of simulated solar light, (b) the contribution of four major subcategories and (c) major classes of compounds separated by black lines in Van Krevelen diagrams of two samples. (CRAM: carboxylic rich alicyclic molecules)

768 **Figure 4**

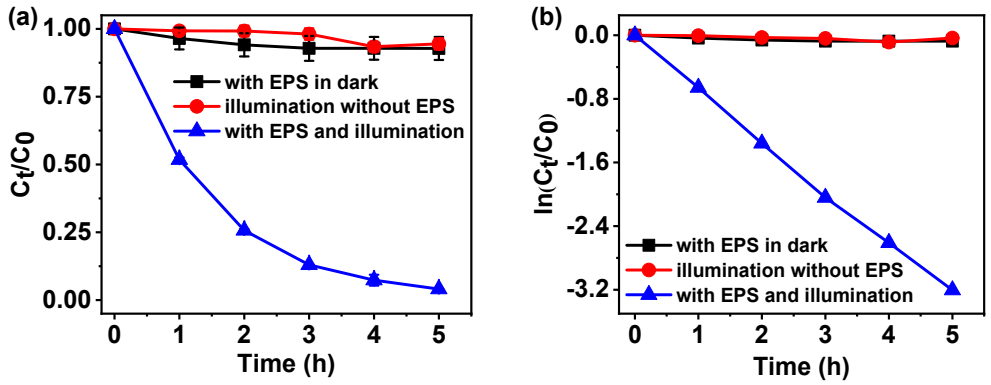

769

770

771 **Figure 4** (a) Efficiency of tetracycline removal during 5-hour illumination. Experimental
772 conditions: [M-EPS] = 20 mg TOC/L and $[TC]_{initial}$ = 40 mg/L in non-buffer solution at 30 ℃
773 (pH ~ 7.0), (b) pseudo-first-order kinetics plotted as $\ln(C_t/C_0)$ as a function of illumination time
774 for TC degradation.

775

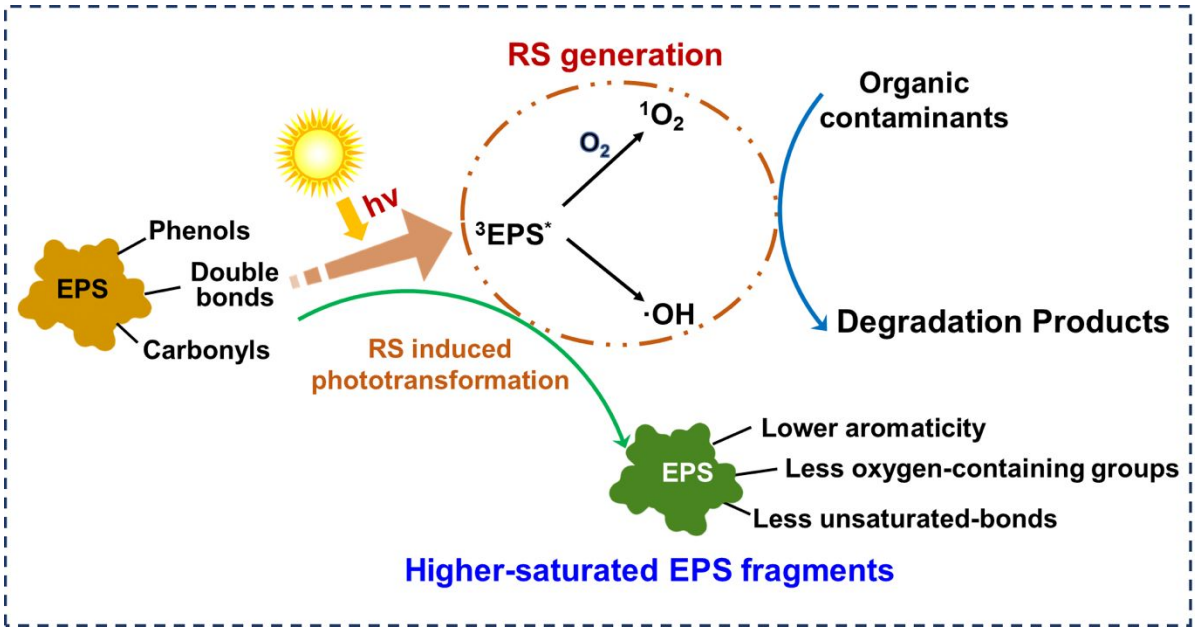

776

777 **Scheme 1** Photochemical behaviors of EPS and its environmental impact.